CrossMark

ARTICLE

Microstructure and flow behavior of cast 2304 duplex stainless steel at elevated temperatures

H. Alinejad,[a] B. Korojy, and G.R. Ebrahimi
Department of Materials and Polymer Engineering, Hakim Sabzevari University, Sabzevar 9617976487, Iran
A. Momeni
Department of Materials Science and Engineering, Hamedan University of Technology, Hamedan 6516913733, Iran

(Received 13 July 2016; accepted 18 November 2016)

Hot deformation characteristics of 2304 duplex stainless steel were analyzed by hot compression tests at temperature range of 850–1150 °C and strain rates of 0.001–1 s^{-1}. The flow curves at low temperatures and high strain rates were suggesting sluggish dynamic recovery (DRV) in ferrite and partial dynamic recrystallization (DRX) in austenite. However, at high temperatures and low strain rates, the flow curves showed implied the domination of DRV in ferrite. The hyperbolic sine equation with activation energy of 508 kJ/mol could relate the processing parameters. Microstructural observations showed that DRV in ferrite is the controlling mechanism at all deformation conditions. However, at high temperatures and strain rates partial DRX could also occur in austenite. Based on the law of mixture and Baragar's equations a modified model was proposed to consider work hardening and dynamic softening in the constituents. The model could satisfactorily predict the flow curves at different deformation regimes.

I. INTRODUCTION

Duplex stainless steels (DSSs) are a class of stainless steels with wide applications in different industries. DSSs are comprised of δ-ferrite and austenite with comparable volume fractions. Since δ-ferrite is more stable at higher temperatures, its content increases with increasing temperature and microstructure becomes fully ferritic at temperatures over 1200 °C.[1–3] Hence, in the hot working temperature range of 900–1200 °C, most of DSSs have a duplex microstructure. The coexistence of austenite and ferrite with different deformation and restoration mechanisms makes it difficult to easily interpret the flow behavior of DSSs through hot or cold working. This complexity has been the motive force for a number of investigations in the past decades.[4–7]

The major source of complexity in the hot deformation behavior of DSSs is that ferrite and austenite have different specific strengths and are softened by different mechanisms. While ferrite undergoes dynamic recovery (DRV),[8–10] austenite tends to soften by dynamic recrystallization (DRX).[11–14] The major difference in the softening behaviors of ferrite and austenite makes it difficult to find a simple model for the flow curves. In other words, the phenomenological and physical-based models, which have been so far developed for single-phase ferritic or austenitic steels, cannot be used to predict the flow behavior of DSSs.

In the past decades, some researchers have tried old constitutive equations such as the hyperbolic sine function for modeling the flow curves of DSSs.[15–17] Other researchers tried to develop new constitutive equations based on the law of mixture rule and the individual behaviors of ferrite and austenite.[18,19] Given the efforts devoted to the issue, the hot deformation behavior of DSSs needs further investigations with the focus on the microstructural evolution and flow curve modeling. Hence, the present investigation aimed at moving forward the current knowledge of the hot deformation behavior of DSSs. In this investigation hot compression tests over a wide range of temperatures and strain rates have been carried out to investigate the microstructural evolution during hot working of 2304 DSS. Moreover, a new constitutive equation has been developed to predict the flow stress at different temperatures and strain rates.

II. MATERIAL AND METHODS

The material used in this study was 2304 DSS with 0.06% C, 21.03% Cr, 4.8% Ni, 0.17% Mo, 0.71% Si, 0.65% Mn, 0.004% S, 0.028% P, and the rest of Fe (all in wt%). The material was cast in a vacuum furnace and then homogenized at 1200 °C for 20 min and quenched to the ambient temperature. The starting microstructure of the material, shown in Fig. 1, was consisted of about 54% ferrite and 45% austenite

Contributing Editor: Jürgen Eckert
[a]Address all correspondence to this author.
e-mail: alinejad.ho@gmail.com
DOI: 10.1557/jmr.2016.457

 © Materials Research Society 2016

https://doi.org/10.1557/jmr.2016.457 Published online by Cambridge University Press

(volume percents). In the micrograph, the matrix is ferrite, in which the austenite islands have been distributed without a specific orientation.

The cylindrical specimens with 10 mm diameter and 15 mm height were prepared from the homogenized cast ingot. Before testing, all specimens were reheated at 1200 °C, held for 5 min and then cooled down at rate of 5 °C/min to testing temperatures. Hot compression tests were performed at temperatures of 850–1150 °C and strain rates of 0.001–1 s^{-1} up to the true strain of 0.5.

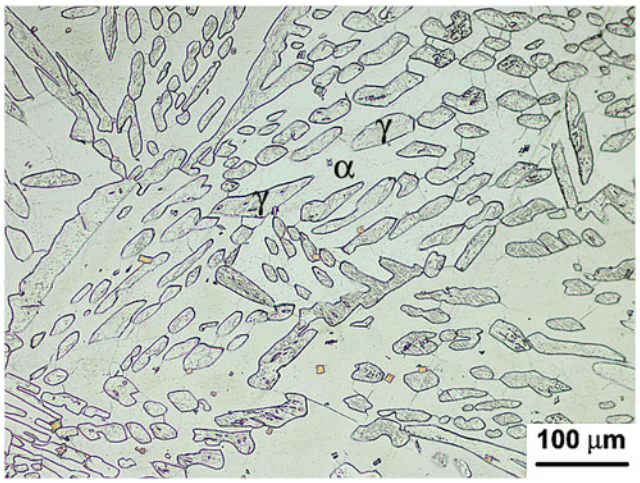


FIG. 1. Starting microstructure of cast 2304 after casting and homogenization. The matrix is ferrite and the darker islands are austenite.

The Zwick-Roell testing machine used in this investigation was equipped with a computer-controlled furnace with the accuracy of ±5 °C. The load–displacement data were recorded by the unit software and then transformed into true stress–strain data by the standard equations. The load cell accuracy was about ±1%. After testing, the hot deformed specimens were quenched within 1–3 s to preserve the microstructures. Graphite powder was applied on both contacting specimen/anvil surfaces to reduce friction coefficient.

For microstructural investigations the hot deformed specimens were cut along their longitudinal axis and the tangential sections were prepared by the standard metallographic techniques. After common grinding and polishing steps, the samples were electrolytically etched in a 40 pct solution of HNO_3 and then characterized by an optical microscope.

III. RESULTS AND DISCUSSION

A. Flow curves and constitutive analysis

Figure 2 demonstrates typical flow curves plotted based on load-stroke data obtained at different deformation conditions. The stress–strain curves clearly indicate the profound effects of temperature and strain rate on the flow behavior. Obviously, at low temperatures and high strain rates, e.g., 850 and 950 °C and strain rates of 0.1 and 1 s^{-1}, flow curves exhibit a moderate work hardening up to a faint peak, which is followed by a gradual flow softening. In the opposite conditions, i.e., high

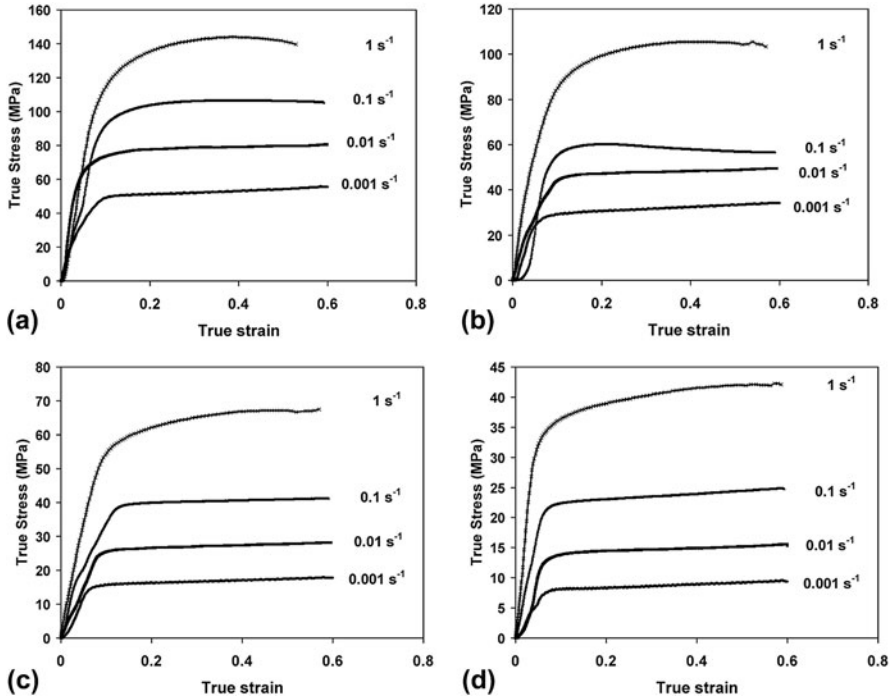


FIG. 2. True stress–true strain curves obtained at different strain rates and temperatures: (a) 850 °C, (b) 950 °C, (c) 1050 °C, and (d) 1150 °C.

https://doi.org/10.1557/jmr.2016.457 Published online by Cambridge University Press

temperatures and low strain rates such as 1050 and 1150 °C and strain rates of 0.001 and 0.01 s^{-1}, the flow curves are characterized by a plateau after work hardening. Such behavior which is typical of DRV indicates that at high temperatures and low strain rates, the material behaves as if only ferrite is present. However, in contrast, at high strain rates and low temperatures, the contribution of austenite is deduced from the peak, which is associated with the start of DRX.[20]

These observations can be simply accounted for by considering the variation of ferrite and austenite volume fractions at different deformation temperatures. According to the phase diagram calculated by the Thermocalc software in Fig. 3, ferrite, austenite (γ and δ), and $M_{23}C_6$ carbides are the microstructural constituents of 2304 (% C = 0.06) in the hot working range (dark rectangle). It should be noted that $M_{23}C_6$ carbide is often formed by aging within the same temperature range[21] and is therefore absent in the present material. The phase diagram also shows that the material becomes fully ferritic at temperatures beyond 1300 °C. Figure 4 indicates a rough calculation of austenite and ferrite volume fractions in the hot working range. It is observed that as temperature rises, the volume fraction of ferrite increases and that of austenite decreases vice versa. Hence, it is easy to understand that why the material behaves as if it is fully ferritic when is deformed at 1050 and 1150 °C.

At low temperatures, especially below 1050 °C, a faint peak appears, representing the initiation of DRX in austenite. It is evident that the peak is more pronounced at high strain rates. Indeed, high strain rates stimulate austenite to take a greater contribution to plastic deformation of DSS. Some works on the individual flow behaviors of ferrite and austenite have shown that there is a considerable difference between the strength levels of these constituents at hot working temperatures.[18,19] As ferrite is the softer phase, it accommodates more strain than austenite. Duprez et al.[3] showed that strain is primarily accommodated by ferrite and then transfers to austenite. The strain transfer is a complicated process which depends on temperature and strain rate. At high temperatures and low strain rates, when ferrite can simply convey large strains due to its expeditious DRV, strain transfer is postponed and austenite can only take a small portion of the total strain. This is clearly understood from the flow curves of Fig. 2 at such conditions. The small strains in austenite do not increase the dislocation density to the critical point for DRX, and therefore the peak is absent. This is why the material behaves as if it is only consisted of ferrite. In contrast, when strain rate rises or temperature decreases, DRV in ferrite degrades and therefore the strain transfer occurs sooner. This gives rise to more accumulation of strain into austenite which finally triggers DRX at the peak.

As the flow stress is not very sensitive to strain, its variation with temperature and strain rate can be described by the familiar hyperbolic sine constitutive equation, given as follows[5]:

$$Z = \dot{\varepsilon} \exp\left(\frac{Q}{RT}\right) = A\ [\sinh(\alpha \cdot \sigma)]^n \quad , \qquad (1)$$

where Z stands for the Zener–Hollomon parameter, which incorporates the effects of strain rate and temperature, Q is the apparent activation energy and A, α, and n

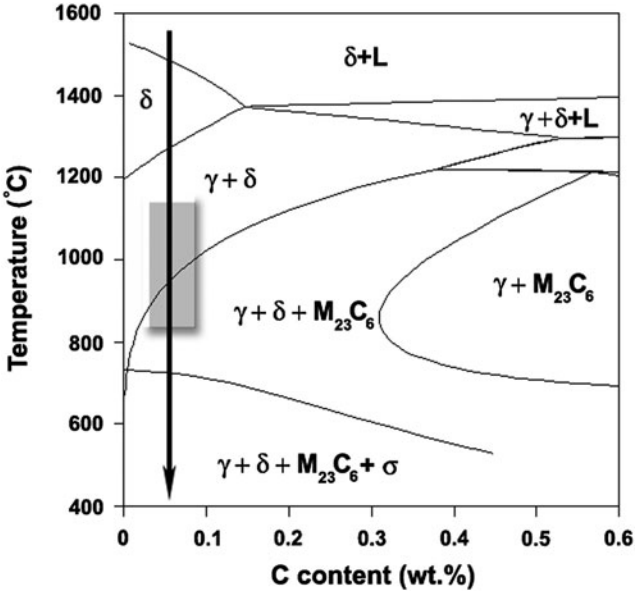


FIG. 3. Phase diagram of the studied alloy calculated by the Thermocalc software, representing the position of the studied alloy by the arrow and the studied hot working range of temperature as a dashed region.

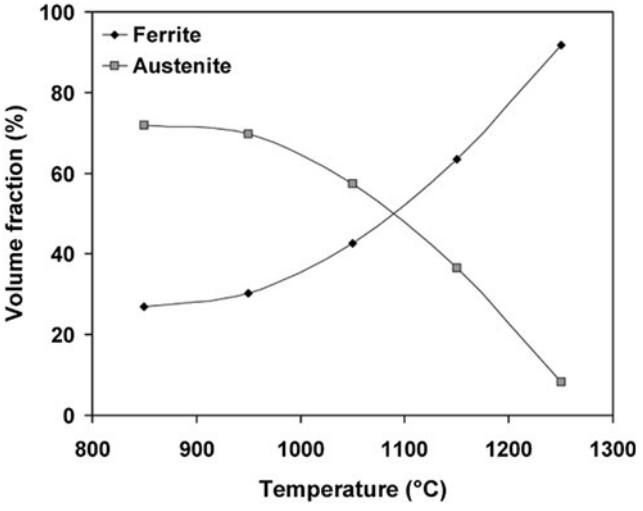


FIG. 4. Variation of ferrite and austenite volume fractions with temperature calculated based on the phase diagram of Fig. 3.

https://doi.org/10.1557/jmr.2016.457 Published online by Cambridge University Press

are the material constants. The materials constants can be determined using the logarithmic form of Eq. (1), given by:

$$\ln \dot{\varepsilon} + \frac{Q}{RT} = \ln A + n \ln[\sinh(\alpha \cdot \sigma)] \quad . \qquad (2)$$

The stress exponent, n, can be determined from the plot of strain rate versus the hyperbolic sine of flow stress (e.g., at $\varepsilon = 0.4$) in a logarithmic scale [Eq. (2)], as illustrated in Fig. 5(a). Similarly, in the plot of $\ln[\sinh(\alpha \cdot \sigma)]$ versus $1/T$ [Fig. 5(b)], Q/nR is the average slope whereby the apparent activation energy can be determined. Based on the adopted method the value of Q is calculated about 508 kJ/mol. It has been proposed that the value of Q for DSSs is often between those of single-phase ferritic and austenitic stainless steels (SSs).[5] This means that the deformation resistance of DSSs is higher than that of ferritic SSs and lower than that of austenitic SSs. On the other words, the high value of Q indicates that flow stress in the studied DSS is highly temperature-dependent.

B. Microstructural observations

As mentioned, the hot deformation behavior of DSSs is complex due to the coexistence of ferrite and austenite. For this reason, the observation of hot deformed microstructures is a key tool to verify and interpret the mechanical testing results which were presented in Sec. II. The influence of deformation temperature on the microstructures deformed at the typical strain rate of 0.1 s^{-1} is observed in Fig. 6. It is observed that the volume fraction of austenite islands has decreased with increase in temperature. This actually decreases the contribution of austenite in the deformation at high temperatures. The observation of none-flattened globular austenite islands is another reason for the low contribution of austenite in the deformed material. In addition, even at 1150 °C, there is no sign of DRX within the austenite islands. It seems that the morphology of austenite may restrict its contribution to the applied strain and therefore its tendency for DRX. It is clear that there are not enough grain boundaries inside the γ islands and the sessile δ/γ phase boundary cannot take part in the nucleation of DRX. In contrast to austenite, the evolutions in ferrite are considerable. The average size of the ferrite grains has clearly increased from about 10 to 15 μm at 850 °C to about 50 μm at 1150 °C. Moreover, the ferrite grains have become sharper at 1050 °C and 1150 °C, which indicates the evolution of the boundaries through the grain growth process. A mechanism such as continuous DRX may be suggested to lead a gradual increase in the misorientation along the boundaries and therefore making them well defined under the microscope.

Figure 7 indicates the effect of strain rate on the microstructures obtained at various deformation temperatures. At all studied temperatures, it is obvious that increasing strain rate from 0.001 to 1 s^{-1} has decreased the average size of the ferrite grains. This is more remarkable at higher temperatures of 1050 and 1150 °C, where the material is subjected to fast grain growth. Indeed, increasing strain rate decreases the deformation time that a sample is subjected to and the finer grain size is r rational result. Another important point is the presence of equiaxed grains in the matrix at all deformation conditions. Based on these observations, it is easily deduced that DRV in ferrite is the major microstructural evolution through the hot deformation of DSSs. Opposite to the evolutions in the matrix, the microstructure of austenite seems to be nearly stable. As mentioned earlier, the major part of the applied strain is accommodated by ferrite and therefore the strain which is carried by the austenite is not enough to propel DRX in this phase. This is nearly the same for all temperatures and strain rates. However, increasing temperature, due to its effect on decreasing the required strain for DRX in austenite, and increasing strain rate, due to increasing the rate of dislocations accumulation, would lead to partial DRX in the austenite.[22] The electron back-scattered diffraction (EBSD) observations carried out by Momeni et al.[17,23] supports this idea; however, the amount of DRX was reported as low as 10%. The micrographs of

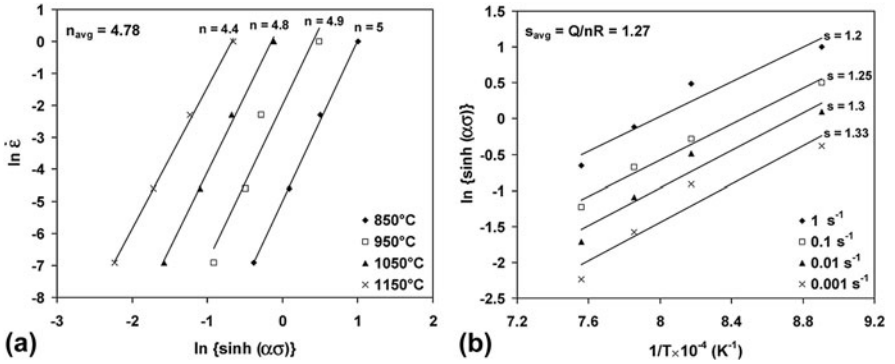


FIG. 5. Variation of the flow stress with (a) strain rate and (b) reciprocal of temperature, in the frame of the hyperbolic sine constitutive equation.

https://doi.org/10.1557/jmr.2016.457 Published online by Cambridge University Press

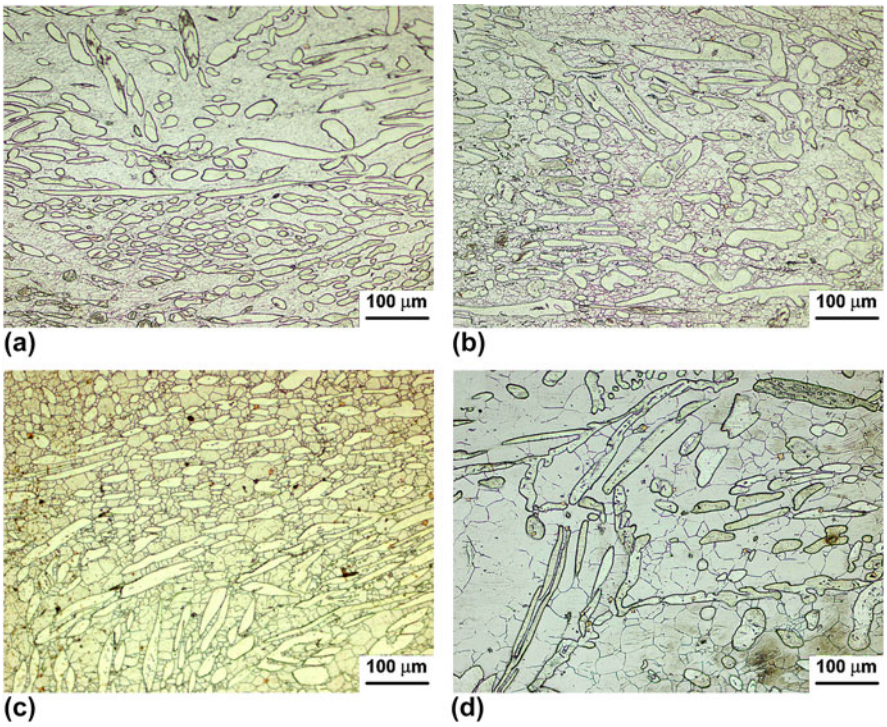


FIG. 6. Micrographs of the hot deformed samples at strain rate of 0.1 s^{-1} and various temperatures: (a) 850 °C, (b) 950 °C, (c) 1050 °C, and (d) 1150 °C.

Figs. 7(f) and 7(h) illustrate some signs of DRX inside the islands which are absent at lower temperatures.

C. A new constitutive equation for modeling the flow curves

As shown in the previous sections, the complexity in DSSs originates from the coexistence of ferrite and austenite with different deformation mechanisms. And this makes it difficult to establish a simple model for predicting the flow curves. Through decades, different constitutive equations have been used to model the flow behavior of single-phase ferritic or austenitic microstructures. The adopted approaches have been divided into two major categories of phenomenological or physics-based models.[24] Some well-known models in each category have been widely investigated for different alloys.[25–27] However, the models which have been used to describe σ(ε), e.g., Kocks-type models[26] or Avrami's kinetics equation,[28] cannot consider concomitant microstructural evolutions such as DRV, DRX, and work hardening in ferrite and austenite. As work hardening is the major part of the microstructural evolution in both phases, it is possible to construct the model based on the simple work hardening equations such as Ludwik's model. Baragar[29] used a modified form of the Ludwik's model to include the effect of other microstructural mechanisms such as DRV during hot working of plain carbon and HSLA steels. The equation proposed by Baragar is presented as follows[29]:

$$\sigma = a + b\varepsilon^{0.4} + c\varepsilon^{0.8} + d\varepsilon^{1.2} \quad , \tag{3}$$

where a, b, c, and d are the material constants. The general form of above equation can be proposed as follows:

$$\sigma = a_1 + a_2\varepsilon^{q} + a_3\varepsilon^{2q} + a_4\varepsilon^{3q} \quad , \tag{4}$$

where a_1 to a_4 and q are the material constants. The most important question that may arise here is that whether Eq. (3) can be used for a duplex structure of austenite and ferrite. To answer this question, we have to verify whether Eq. (3) is capable to describe the flow behaviors of ferrite and austenite separately.

The flow behavior of ferrite in DSSs is often described by the Kocks model[26] which is constructed based on the dislocation evolution law during work hardening and DRV. The Kock's model is finalized to the following description of σ(ε):

$$\sigma = \sigma_s + (\sigma_s - \sigma_0)\exp(-r\varepsilon) \quad , \tag{5}$$

where σ_s and σ_0 are the saturated and yield stress and r is the recovery factor. Assuming $\sigma_s \gg \sigma_0$, Eq. (5) can be simplified as follows:

$$\sigma = \sigma_s[1 + \exp(-r\varepsilon)] \quad . \tag{6}$$

https://doi.org/10.1557/jmr.2016.457 Published online by Cambridge University Press

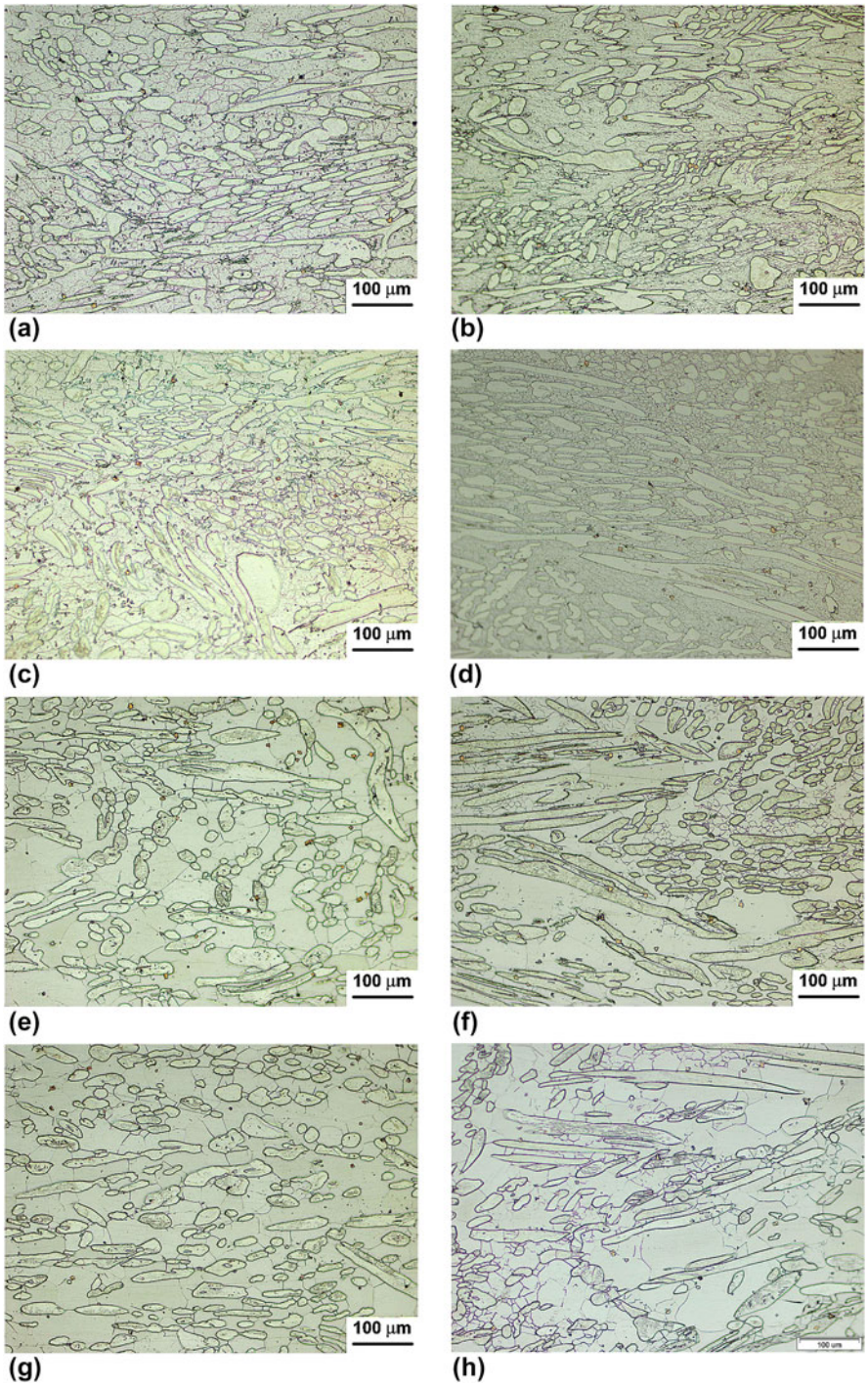


FIG. 7. Micrographs of the hot deformed samples at (a) 850 °C-0.001 s^{-1}, (b) 850 °C-1 s^{-1}, (c) 950 °C-0.001 s^{-1}, (d) 950 °C-1 s^{-1}, (e) 1050 °C-0.001 s^{-1}, (f) 1050 °C-1 s^{-1}, (g) 1150 °C-0.001 s^{-1}, and (h) 1150 °C-1 s^{-1}.

By using the Taylor series for the exponential function $(1 + x + x^2/2! + x^3/3! + \ldots)$, Eq. (6) can be rewritten as:

$$\sigma = \sigma_s \left[2 - r\varepsilon + \frac{1}{2}(r\varepsilon)^2 - \frac{1}{6}(r\varepsilon)^3 \right] \quad . \qquad (7)$$

It is obvious that Eq. (7) is a version of Eq. (4) with $q = 1$. It is therefore concluded that Eq. (4) in its general form is able to consider the flow behavior of ferrite in a DSS. To establish a formulation for the flow behavior of austenite, we can start with the equation proposed by Cingara and McQueen[30] as follows:

https://doi.org/10.1557/jmr.2016.457 Published online by Cambridge University Press

$$\frac{\sigma}{\sigma_p} = \left[(\varepsilon/\varepsilon_p)\exp(1-\varepsilon/\varepsilon_p)\right]^C \quad , \tag{8}$$

where C is a material constant and σ_p and ε_p denotes the peak stress and strain of a typical DRX flow curve. This equation can satisfactorily model the flow curve of austenite even up to the early stages of DRX. Yazdani et al.[31] showed that the value of c determines the rate of work hardening and can vary between 0.2 and 0.85. Using the Taylor series for the exponential function and doing some algebraic operations, Eq. (8) can be simplified as follows:

$$\frac{\sigma}{\sigma_p} = \left[2.5\left(\frac{\varepsilon}{\varepsilon_p}\right) - 2\left(\frac{\varepsilon}{\varepsilon_p}\right)^2 + 0.5\left(\frac{\varepsilon}{\varepsilon_p}\right)^3\right]^C \quad . \tag{9}$$

The final step in this sequence is to calculate the flow stress of the DSS using the law of mixture rule, which has been applied for different two-phase alloys such as leaded brasses or stainless steels[32]:

$$\sigma_{DSS} = f_\gamma \sigma_\gamma + f_\alpha \sigma_\delta \quad , \tag{10}$$

where f stands for the volume fraction and subscripts γ and δ refer to austenite and ferrite, respectively. If Eqs. (7), (9), and (10) are combined; the flow stress of a DSS can be proposed as follows:

$$\sigma_{DSS} = f_\gamma \sigma_p \left[2.5\left(\frac{\varepsilon}{\varepsilon_p}\right) - 2\left(\frac{\varepsilon}{\varepsilon_p}\right)^2 + 0.5\left(\frac{\varepsilon}{\varepsilon_p}\right)^3\right]^C + f_\alpha \sigma_s \left[2 - r\varepsilon + \frac{1}{2}(r\varepsilon)^2 - \frac{1}{6}(r\varepsilon)^3\right] \quad . \tag{11}$$

It is obvious that Eq. (11) can be simplified to the general form of Baragars's equation, given by Eq. (3). This approach proves that the Baragars's equation is capable to take both the flow cures of ferrite and austenite into consideration and incorporate them into a single simple equation for any DSS. Equations (3) and (11) show that a, b, c, and d are the material constants which are functions of σ_p and ε_p (for austenite), σ_s and r (for ferrite), f_γ and f_δ.

Based on Eq. (3), by taking p equal to 0.4, the least square fitting method can be used to calculate the material constants a, b, and c at different deformation conditions. As mentioned, the material constants a, b, and c are functions of σ_p and ε_p (for austenite), σ_s and r (for ferrite), f_γ and f_δ and they can be related to the deformation temperature and strain rate or the Z parameter. Figure 8 shows the variations of a, b, c, and d with the Z parameter.

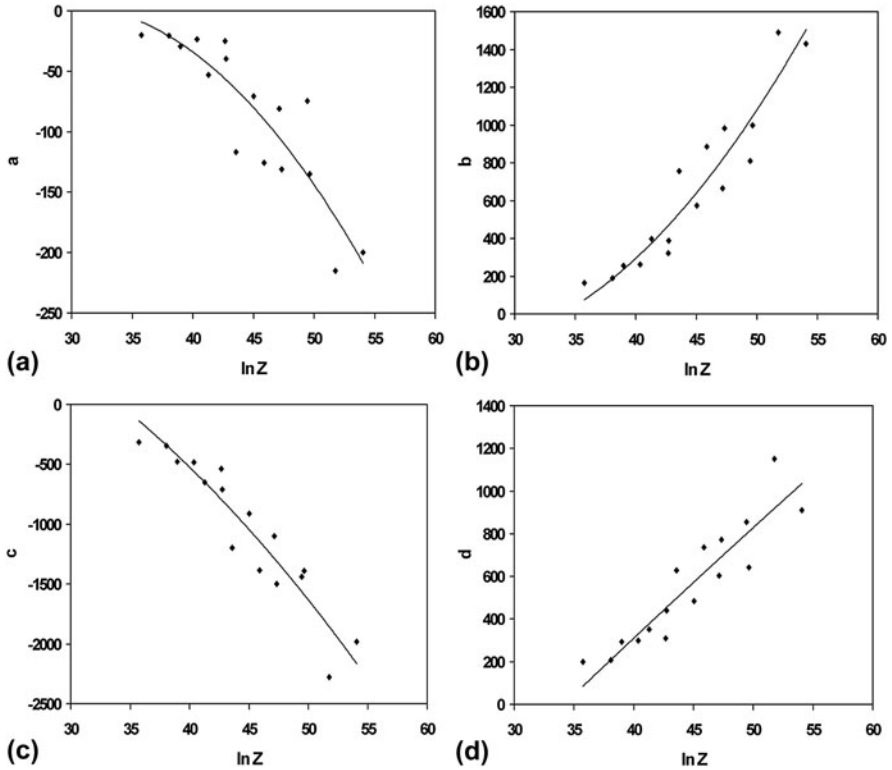


FIG. 8. Materials constants a, b, c, and d [in Eq. (4)] as functions of the Zener–Hollomon parameter. The curves give the polynomial fitting of experimental data.

https://doi.org/10.1557/jmr.2016.457 Published online by Cambridge University Press

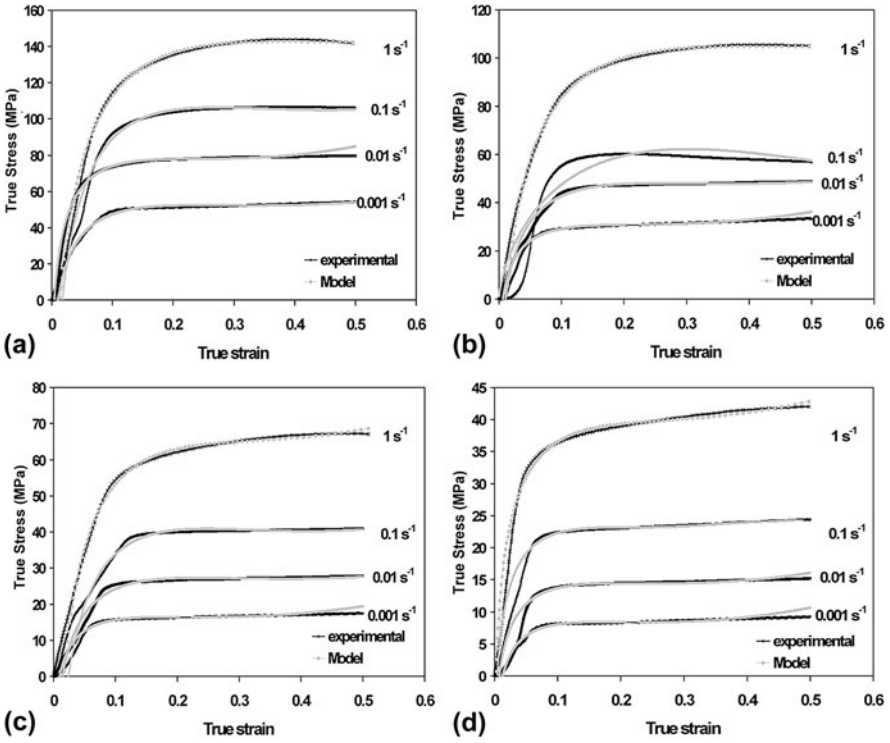


FIG. 9. Comparison of the experimental flow curves and those calculated using the established constitutive equation in Eq. (12): (a) 850 °C, (b) 950 °C, (c) 1050 °C, and (d) 1150 °C.

The values of Z were determined using the method described in Sec. III. A. It is observed that polynomial curves well define the relationship between the constants and Z. By using the predicted values of the constants and replacing into Eq. (11) the modeled curves were calculated and superimposed on the experimental ones in Fig. 9. It is manifest that the model developed based on the Baragar's equation can satisfactorily predict the experimental flow curves.

IV. CONCLUSIONS

The hot deformation characteristics of cast 2304 DSS were analyzed by the constitutive equations and microstructural observations. The major results are listed below:

(1) The flow curves at low temperatures and high strain rates are characterized by moderate work hardening up to a faint peak followed by a moderate work softening. All these were attributed to the sluggish DRV in ferrite and partial DRX in austenite.

(2) At high temperatures and low strain rates, the flow curves were characterized by a long plateau after primary work hardening, representing the expeditious DRV in ferrite.

(3) The hyperbolic sine constitutive equation was used to establish a relationship between flow stress and the Zener–Hollomon parameter. The value of apparent activation energy was calculated as 508 kJ/mol.

(4) The microstructural observations confirmed that DRV in ferrite occurs at all temperatures and strain rates. However, the DRX in austenite partly occurs at high temperatures and high strain rates.

(5) A new constitutive equation was proposed based on the flow behaviors of ferrite and austenite and the law of mixture rule. The proposed equation was constructed based on the Baragar's model to consider work hardening and DRV in the constituent phases. The proposed model satisfactorily predicts the flow curves at different deformation regimes.

REFERENCES

1. H. Keshmiri, A. Momeni, K. Dehghani, G.R. Ebrahimi, and G. Heidari: Effect of aging time and temperature on mechanical properties and microstructural evolution of 2205 ferritic–austenitic stainless steel. *J. Mater. Sci. Technol.* **25**, 597 (2009).
2. Y.L. Fang, Z.Y. Liu, H.M. Song, and L.Z. Jiang: Hot deformation behavior of a new austenite–ferrite duplex stainless steel containing high content of nitrogen. *Mater. Sci. Eng., A* **526**, 128 (2009).
3. L. Duprez, B.C. De Cooman, and N. Akdut: Flow stress and ductility of duplex stainless steel during high-temperature torsion deformation. *Metall. Mater. Trans. A* **33**, 1931 (2002).
4. O. Balancin, W.A.M. Hoffmann, and J.J. Jonas: Influence of microstructure on the flow behavior of duplex stainless steels at high temperatures. *Metall. Mater. Trans. A* **31**, 1353 (2000).
5. H. Farnoush, A. Momeni, K. Dehghani, J. Aghazadeh Mohandesi, and H. Keshmiri: Hot deformation characteristics of 2205 duplex stainless steel based on the behavior of constituent phases. *Mater. Des.* **31**, 220 (2010).

https://doi.org/10.1557/jmr.2016.457 Published online by Cambridge University Press

6. K.R. Gadelrab, G. Li, M. Chiesa, and T. Souier: Local characterization of austenite and ferrite phases in duplex stainless steel using MFM and nanoindentation. *J. Mater. Res.* **27**, 1573 (2012).
7. Y. Han, D. Zou, Z. Chen, G. Fan, and W. Zhang: Investigation on hot deformation behavior of 00Cr23Ni4N duplex stainless steel under medium–high strain rates. *Mater. Charact.* **62**, 198 (2011).
8. P. Mao, K. Yang, and G. Su: Hot deformation behavior of an as-cast duplex stainless steel. *J. Mater. Sci. Technol.* **19**, 379 (2003).
9. H.J. McQueen, N.D. Ryan, E. Evangelista, and X. Xia: Flow stresses, grain and subgrain structures developed by hot working in as-cast 409 stainless steel. *Proc. 34th Mechanical Working and Steel Processing*, Iron and Steel Inst. AIME, Warrendale, 1993; p. 101.
10. P. Cizek and B.P. Wynne: A mechanism of ferrite softening in a duplex stainless steel deformed in hot torsion. *Mater. Sci. Eng., A* **230**, 88 (1997).
11. A. Momeni, G.R. Ebrahimi, M. Jahazi, and P. Bocher: Microstructure evolution at the onset of discontinuous dynamic recrystallization: A physics-based model of subgrain critical size. *J. Alloys Compd.* **587**, 199 (2014).
12. H. Zhang, K. Zhang, S. Jiang, and Z. Lu: The dynamic recrystallization evolution and kinetics of Ni–18.3Cr–6.4Co–5.9W–4Mo–2.19Al–1.16Ti superalloy during hot deformation. *J. Mater. Res.* **30**, 1029 (2015).
13. A. Momeni, S.M. Abbasi, M. Morakabati, H. Badri, and X. Wang: Dynamic recrystallization behavior and constitutive analysis of Incoloy 901 under hot working condition. *Mater. Sci. Eng., A* **615**, 51 (2014).
14. Y.C. Lin, X.Y. Wu, X.M. Chen, J. Chen, D.X. Wen, J.L. Zhang, and L.T. Li: EBSD study of a hot deformed nickel-based superalloy. *J. Alloys Compd.* **640**, 110 (2015).
15. A. Momeni and K. Dehghani: Hot working behavior of 2205 austenite–ferrite duplex stainless steel characterized by constitutive equations and processing maps. *Mater. Sci. Eng., A* **528**, 1448 (2011).
16. J.M. Cabrera, A. Mateo, L. Llanes, J.M. Prado, and M. Anglada: Hot deformation of duplex stainless steels. *J. Mater. Process. Technol.* **143–144**, 321 (2003).
17. A. Momeni, K. Dehghani, and X.X. Zhang: Mechanical and microstructural analysis of 2205 duplex stainless steel under hot working condition. *J. Mater. Sci.* **47**, 2966 (2012).
18. S. Spigarelli, M. El Mehtedi, M. Cabibbo, F. Gabrielli, and D. Ciccarelli: Constitutive equations for prediction of the flow behaviour of duplex stainless steels. *Mater. Sci. Eng., A* **615**, 331 (2014).
19. A. Momeni, K. Dehghani, and M.C. Poletti: Law of mixture used to model the flow behavior of a duplex stainless steel at high temperatures. *Mater. Chem. Phys.* **139**, 747 (2013).
20. Y. Liu, Y. Ning, Z. Yao, Y. Li, J. Zhang, and M. Fu: Dynamic recrystallization and microstructure evolution of a powder metallurgy nickel-based superalloy under hot working. *J. Mater. Res.* **31**, 2164 (2016).
21. I. Zucato, M.C. Moreira, I.F. Machado, and S.M. Giampietri Lebrão: Microstructural characterization and the effect of phase transformations on toughness of the UNS S31803 duplex stainless steel aged treated at 850 °C. *Mater. Res.* **5**, 385 (2002).
22. M.S. Chen, Y.C. Lin, and X.S. Ma: The kinetics of dynamic recrystallization of 42CrMo steel. *Mater. Sci. Eng., A* **556**, 260 (2012).
23. A. Momeni, S. Kazemi, and A. Bahrani: Hot deformation behavior of microstructural constituents in a duplex stainless steel during high-temperature straining. *Int. J. Miner., Metall. Mater.* **20**, 953 (2013).
24. Y.C. Lin and X-M. Chen: A critical review of experimental results and constitutive descriptions for metals and alloys in hot working. *Mater. Des.* **32**, 1733 (2011).
25. G.R. Johnson and W.H. Cook: A constitutive model and data for metals subjected to large strains, high strain rates and high temperatures. *7th International Symposium on Ballistics*, Den Haag, Netherlands, 1983; p. 541.
26. U.F. Kocks: Laws for work-hardening and low-temperature creep. *J. Eng. Mater. Technol.* **98**, 76 (1976).
27. Y.C. Lin and X.M. Chen: A combined Johnson–Cook and Zerilli–Armstrong model for hot compressed typical high-strength alloy steel. *Comput. Mater. Sci.* **49**, 628 (2010).
28. J.J. Jonas, X. Quelennec, L. Jiang, and E. Martin: The Avrami kinetics of dynamic recrystallization. *Acta Mater.* **57**, 2748 (2009).
29. D.L. Baragar: The high temperature and high strain rate behavior of plain carbon and an HSLA steel. *J. Mech. Work. Technol.* **14**, 295 (1987).
30. A. Cingara and H.J. McQueen: New formula for calculating flow curves from high temperature constitutive data for 300 austenitic steels. *J. Mater. Process. Technol.* **36**, 31 (1992).
31. M. Yazdani, S.M. Abbasi, A. Karimi Taheri, and A. Momeni: Hot deformation behavior of Fe–29Ni–17Co alloy. *Trans. Nonferrous Met. Soc. China* **23**, 3271 (2013).
32. A. Momeni: Application of a self-consistent model to study the flow behavior of CuZn39Pb3 at elevated temperatures. *J. Mater. Res.* **30**, 3453 (2015).

https://doi.org/10.1557/jmr.2016.457 Published online by Cambridge University Press